Graded Yb:YAG ceramic structures: design, fabrication and characterization of the laser performances

Guido Toci[a*], Antonio Lapucci[b], Marco Ciofini[b], Laura Esposito[c], Jan Hostaša[c,f], Andreana Piancastelli[c], Leonida A. Gizzi[d], Luca Labate[d], Paolo Ferrara[d], Angela Pirri[e], Matteo Vannini[a]
a) CNR – INO National Research Council, Istituto Nazionale di Ottica, Via Madonna del Piano 10, I-50019 Sesto Fiorentino (FI) Italy
b) CNR - INO National Research Council, Istituto Nazionale di Ottica, Largo Enrico Fermi 6, I-50125 Firenze, Italy
c) CNR - ISTEC National Research Council, Institute of Science and Technology for Ceramics, Via Granarolo 64, 48018 Faenza, Italy
d) CNR - INO National Research Council, Istituto Nazionale di Ottica, Via G. Moruzzi, 1 - I-56124 Pisa, Italy;
e) CNR - IFAC National Research Council, Institute of Applied Physics "Nello Carrara", Via Madonna del Piano 10, I-50019 Sesto Fiorentino (FI) Italy
f) Department of Glass and Ceramics, Institute of Chemical Technology, Prague, 166 28 Prague 6, Czech Republic

ABSTRACT

Significant improvements in efficiency in high power, high repetition rate laser systems should come from the use of ceramic laser active elements suitably designed to mitigate the thermal and thermo-mechanical effects (TEs and TMEs) deriving from the laser pumping process. Laser active media exhibiting a controlled and gradual distribution of the active element(s) could therefore find useful applications in the laser-driven inertial confinement fusion systems, which are considered among the most promising energy source of the future (ultraintense laser pulses), and in medical applications (ultrashort laser pulses)
The present work explores the flexibility of the ceramic process for the construction of YAG ($Y_3Al_5O_{12}$) ceramic laser elements with a controlled distribution of the Yb doping, in view of the realization of structures modelled to respond to specific application. Two processing techniques are presented to prepare layered structures with a tailored modulation of the doping level, with the goal of reducing the peak temperature, the temperature gradients and also the thermally-induced deformation of the laser material, thus mitigating the overall thermal effects. Tape casting in combination with thermal compression of ceramic tapes with a varying doping level is one of the presented techniques. To make this process as more adaptable as possible, commercial micrometric ceramic powders have been used. The results are compared with those obtained using nanometric powders and a shaping process based on the subsequent pressing of spray dried powders with a different doping level. Laser performance has been characterized in a longitudinally diode pumped laser cavity. The laser efficiency under high thermal load conditions has been compared to those obtained from samples with uniform doping, and for samples obtained with press shaping and tape casting, under the same conditions.

Keywords: Lasers and laser optics, Lasers, solid state, Lasers, diode pumped, Thermal effects, Lasers, Ytterbium, Ceramic lasers, Graded doping, Tape casted ceramics.

1. INTRODUCTION

Ceramic-based materials have shown to be a competitive alternative to single crystals for solid state lasers especially in case of high power applications[1]. The ceramic process is highly flexible in terms of feasible geometries and shapes, as well as dopant distribution control. This approach allows the implementation of technical solutions which are unfeasible or very difficult to implement with the current crystal growth and fabrication technologies.
The current level of development of transparent YAG ceramics gives them a laser performance fully comparable with their crystalline counterpart [2,3]. Ceramics also have specific advantages over single crystals that can be useful in

*guido.toci@ino.it; phone +39-0555225315. www.ino.it

High-Power, High-Energy, and High-Intensity Laser Technology II, edited by Joachim Hein, Proc. of SPIE Vol. 9513, 95130R · © 2015 SPIE
CCC code: 0277-786X/15/$18 · doi: 10.1117/12.2178364

developing certain applications. In particular, when using high doping levels, a more uniform dopant distribution can be achieved. Moreover YAG ceramics exhibit better mechanical properties than their crystalline equivalent [4].
One of the key aspects for producing high power laser sources and amplifiers based on ceramic active media is the management of the thermal effects (TEs) and thermo-mechanical effects (TMEs) (*e.g.* thermal lens, stress-induced depolarization, surface deformations) deriving from the laser pumping process. These effects can degrade the performance of the laser source and can eventually lead to a catastrophic failure of the laser active element.
In this frame, we have investigated the issues related to the design, the production process and the characterization of the laser emission properties of Yb:YAG ceramic elements. Complex shapes and structured doping have been proposed, for the mitigation of the TEs and TMEs in specific laser pumping and cooling geometries.
Regarding the fabrication, we have explored the possibilities offered by the tape casting technique used in combination with thermal compression of ceramic tapes. With this technique it is possible to assemble several tapes with a different composition, press them at a moderate temperature and after the proper thermal treatments obtain graded structures with a changing composition in one direction.
To exploit the potentialities of this process, planar structures of Yb:YAG with longitudinal distribution of Yb concentration were designed and optimized by means of simulations based on Finite Elements Analysis, for the evaluation of their thermal and thermo-mechanical behavior under various pumping and cooling configurations. The simulations show[5] that by this approach an effective reduction of the internal thermo-mechanical stress can be obtained with respect to homogeneous structures operating in the same configuration.

2. MATERIAL FABRICATION

The samples were prepared both with the tape cast and the hot pressing techniques, with two different doping profiles:
- a stepped profile, with two layers having 0% Yb doping and 10% Yb doping;
- a graded profile, with four layers with 7%, 5%, 3%, 1% Yb, doping (Tables 1 and 2);
Individual layer thicknesses and overall samples thicknesses are reported in Table 2.
Seven compositions reported in Table 1 have been selected and prepared by tape casting and spray drying. Table 2 summarizes the compositions selected for the preparation of the structured samples. In the following sections the experimental procedure used for the preparation of the samples is reported.

Chemical formula	Yb^{3+} content with respect to the total amount of Y (at %)	Yb^{3+} content with respect to all elements (at %)
$Y_3Al_5O_{12}$	0	0
$Yb_{0.03}Y_{2.97}Al_5O_{12}$	1	0.15
$Yb_{0.09}Y_{2.91}Al_5O_{12}$	3	0.45
$Yb_{0.15}Y_{2.85}Al_5O_{12}$	5	0.75
$Yb_{0.21}Y_{2.79}Al_5O_{12}$	7	1.05
$Yb_{0.30}Y_{2.70}Al_5O_{12}$	10	1.50

Table 1. Stoichiometry of the selected compositions.

Sample n.	Composition at % Yb YAG	Processing technique	Overall Thicknesses mm	Thickess of single layers mm
TC-1	0-10	Tape casting & thermal compression	1.9	1.0 (Undoped) 0.9 (10 at % Yb)
TC-2	1-3-5-7	Tape casting & thermal compression	2.0	0.5
SD-1	0-10	Pressing of spray dryed powders	3.6	1.6 (Undoped) 2.0 (10 at % Yb)
SD-2	1-3-5-7	Pressing of spray dryed powders	2.0	0.5

Table 2. Composition and structure of tested samples.

Powder (process)	Producer, type	Purity	Mean grain size [μm]
Al_2O_3 (TC, SD)	TM-DS-6, Taimei Chemicals, Japan	> 99.99 %	0.2
Y_2O_3 (TC)	REacton®, Alfa Aesar, MA, USA	> 99.99 %	3.9
Y_2O_3 (SD)	Nanocerox, MI, USA	> 99.99 %	0.05
Yb_2O_3 (TC, SD)	REacton®, Alfa Aesar, MA, USA	> 99.99 %	5.6

Table 3. Characteristics of the starting oxide powders used for the tape casting (TC) and spray drying and pressing (SD) processes.

High-purity oxide powders were used in both processes (their characteristics are listed in Table 3) and TEOS (tetraethyl orthosilicate) was used as sintering additive (0.5 wt %). The preparation of samples TC-1 and TC-2 reported in Table 2 started with the tape casting of sheets (approximately 100 μm thick) with the compositions reported in Table 1. Slurries were prepared according to the procedures and formulations reported by Mistler *et al.*[6]: the powders were wet ball milled for 24 hours using an azeotropic mixture of methyl ethyl ketone and ethanol with TEOS as sintering additive, and the organic additives (dispersant, plasticizer and binder) were added in subsequent steps. Disks with a diameter of 40 mm were cut from the sheets and assembled together by thermal compression at 100 C.

Samples SD-1 and SD-2 (Table 2) were prepared by dry pressing of spray dried powders (Table 3). The oxide powders were mixed with ethanol and TEOS by ball milling for 72 h with 99.9% Al_2O_3 milling media. 1 wt % of polyethylene glycol (PEG 400) was added as an organic dispersant that helps the mutual sliding of the particles during the shaping by pressing. The suspension was then granulated by spray drying in a Mini Spray Dryer B-290 (Büchi Labortechnik AG, Switzerland); the process is described more in detail in [7,8]. Pellets 15 mm in diameter and about 1 mm thick were then obtained by separate uniaxial pressing of each granulated powders. The layered samples were prepared by (linear and cold isostatic) pressing of the thin pellets appropriately assembled to obtain the samples SD-1 and SD-2. For comparison, a sample with a homogeneous 10 at % Yb:YAG composition and an undoped YAG sample were also prepared

All the prepared samples were treated in air at 600 °C for the removal of the organic additives. Sintering was conducted under high vacuum (10^{-4} Pa) in a clean, carbon-free furnace at 1735°C with 16 h soaking time. After sintering, the materials contain oxygen vacancies, which cause light scattering and a grey coloration, and the Yb^{3+} ions are reduced to Yb^{2+}, giving the material a green color. Because Yb^{3+} ions are needed for the laser action, the materials subsequently had to be re-oxidized, so the samples were annealed at 1100°C in air for 100 h. Finally, the sintered samples were then polished with diamond pastes and sprays up to 0.25 μm.

3. NUMERICAL SIMULATIONS

To understand the thermal and thermo-mechanical effects induced by the optical pumping in samples with different doping distributions we performed several numerical simulations making use of a commercial Our approach is based on the adoption of a commercial F.E.M. (Finite Element Mesh Calculation Method) software package [9]. In this paragraph we present the results obtained using heat loading distributions and thermal boundary conditions as close as possible to the experiment reported in this paper. Three different doping distributions are compared: uniform (5%), graded (1-3-5-7%) and stepped (0-10%). Our software package output consists in a scalar temperature variation field $\Delta T=T- T_{REF}$, the geometrical displacements of each node of the mesh and, finally, the 6 components of the stress tensor (σ_i and τ_{ij}). An example of the results of these numerical simulations is shown in Figure 1.

These data give an immediate information on some operational features of the different samples as laser active media. The maximum internal stress at a given power loading is, for instance, an indicator of how far we are working from the "fracture limit". Furthermore they can be used to calculate thermo-optical effects such as thermal lens or stress induced depolarization.

The thermal lens can be calculated considering that the Optical Path Difference (OPD) at different transverse positions is related to three contributions [10]: the refractive index variations with temperature, the surface bending due to thermal expansion and the stress induced birefringence due to the photo-elastic effect:

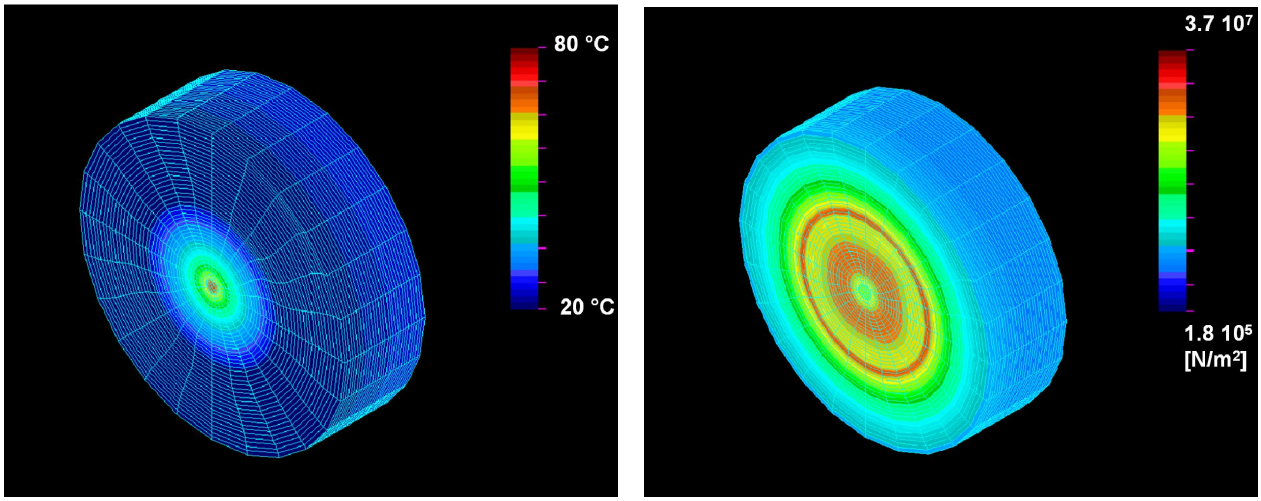

Figure 1. Examples of three dimensional plots of the FEM software output: Temperatures (Left) and Von Mises Stress (Right). Color online.

$$OPD(r) = \left(\int_0^d \frac{dn}{dT} \cdot \Delta T(r,z) dz \right) + n_0 \cdot \Delta u(r) + \left(\sum_{i,j=1}^{3} \int_0^d \frac{\partial n}{\partial \varepsilon_{ij}} \cdot \varepsilon_{ij}(r) dz \right) \quad (1)$$

where d is the sample thickness , n_0 is the refractive index without deformations, $\Delta u(r)$ is the surface deformation at radial position r, and ε_{ij} is the strain tensor. In what follows z is the direction parallel to the cylindrical axis and to the "optical rays propagation".

To determine stress induced effects we need the relation between the refractive index (for the different polarization directions) and the strain tensor. This relation is in general expressed by a variation of the dielectric permeability 2nd rank tensor B_{ij} [11] and is given by the set of equations:

$$\Delta B_{ij} = p_{ijkl} \varepsilon_{kl} \quad (2)$$

$$\Delta n_i - \frac{n_0^3}{2} \cdot \Delta B_{ii}^* \quad (3)$$

where p_{ijkl} is the 4th rank elasto-optical tensor, n_i are the refractive indices along the principal axes of the stress-perturbed indicatrix [12] and ΔB_{ij}^* is the diagonalized dielectric impermeability variation tensor. Fortunately equation (3) reduces to a much simpler formulation in case of a cubic crystal with [111] orientation. Moreover Khazanov [13] demonstrated that the YAG ceramic behavior is similar to that of the [111] oriented single crystal, given the averaging effect of the different grains orientations.

Parameter	*Uniform*	*Graded*	*Stepped*
Maximum Temperature	71°C	65°C	81°C
Maximum Von Mises Stress	3.0 *10^{-7} N/m^2	2.9 *10^{-7} N/m^2	3.7 *10^{-7} N/m^2
Front surface sag (pump side)	3.6 * 10^{-8} m	2.5 * 10^{-8} m	0.5 * 10^{-8} m
Rear Surface sag (cooler side)	1.9 * 10^{-8} m	3.0 * 10^{-8} m	3.4 * 10^{-8} m
Total Thermal Lens	8.2 cm	8.5 cm	8.5 cm

Table 4 - Peak temperature, peak stress level, surface deformation and thermal lens values resulting from the simulations on the various structures.

Table 4 summarizes the results for the three cases of interest in this paper, namely the uniform, graded and stepped cases. We can immediately note that the different doping distributions determine an almost irrelevant change in the total thermal lens observed in the three cases. This is simply understood considering the substantially radial cooling and the averaging effect of propagation on a direction parallel to the doping gradients. The propagation gives origin to the z-

integration in Eq.1 that produces this substantial independence of the total thermal lens from different longitudinal doping distributions. Only the surface deformation contribution to the thermal lens is affected (resulting lower in cases with lower doping close to the surfaces). But this contribution is almost irrelevant for our geometry case-study. Nevertheless, even in our case, doping ramps result effective in reducing the internal temperature and stresses thus indicating the possibility of higher pump loading under the stress limit threshold.
Different conclusions are drawn, of course, for different geometries [5, 10] such as that of thin face cooled disk lasers. Here the surface deformation contribution to the thermal lens results much more relevant and doping distributions variations became relevant also for the control of this deleterious effect.

4. EXPERIMENTAL SETUP FOR LASER TESTS

The samples were tested in the laser cavity shown in Figure 2. The cavity is longitudinally pumped through its flat end mirror EM, which is dichroic whit a high transmission at the pump wavelength and a high reflection at the lasing wavelengths. As a pump source we used a fiber coupled diode laser emitting at 936 nm, with a fiber core diameter of 200 microns and numerical aperture 0.22. The fiber output was refocused into the sample by a pair of achromatic doublets, through the cavity end mirror. The maximum pump power delivered to the sample was about 21W. The pump beam had an almost Gaussian profile with a diameter of 260 μm @ $1/e^2$ of the peak intensity. The deviation from a top-hat profile is due to the residual lens aberrations.
The cavity was V-shaped, with a folding mirror FM having a curvature radius of 100 mm set at a small incidence angle, and a flat output coupler OC. The lengths of the cavity arms were D1=62 mm and D2=260 mm respectively. The calculated size of the TEM_{00} mode cavity beam waist on the mirror EM is w_0=40 μm on the tangential plane and 44 μm for the sagittal plane, for the "cold" cavity. The samples were uncoated, and they were carefully oriented so as to reinject the Fresnel reflection at the surfaces back on the cavity axis, in order to minimize reflection losses. The samples were placed very near to the EM (less than 1 mm between the sample input face and the EM), as shown in the pictures of Figure 3.

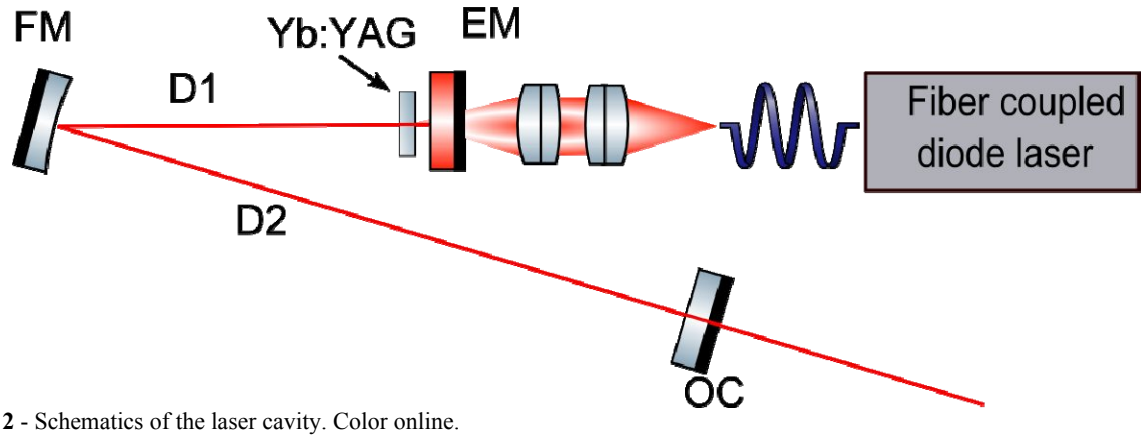

Figure 2 - Schematics of the laser cavity. Color online.

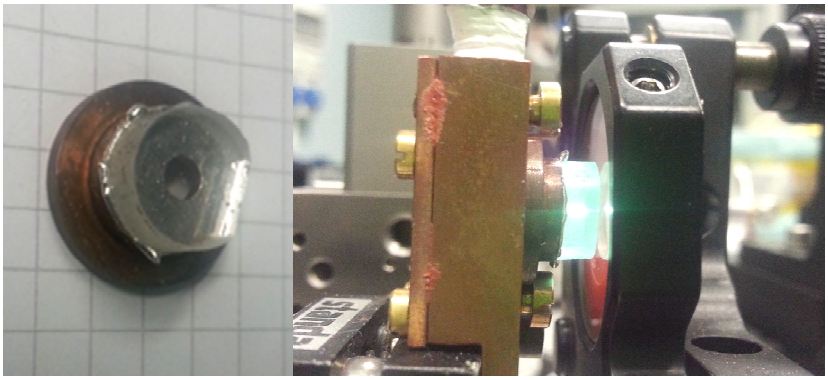

Figure 3 - Left: typical arrangement of the samples soldered of the copper heat sink. Right: the sample under pumping in the laser cavity, set near to the end mirror EM (this latter is on the right side of the picture). Color online.

We used different values of transmission of the output coupler (OC) to find the best coupling conditions.
The samples were cooled by contact with a copper heat sink, where the sample is soldered with Indium. The copper heat sink has a central window to let the laser and pump beams pass through. The samples were joined to the heat sink on the side with the highest doping, whereas the pump beam enters from the side with the lowest doping. This arrangement, enlightened in Figure 4, ensures that the highest power dissipation density occurs on the side nearest to the heat sink.
The crystal holder was placed on a 3-axis micrometric translator, allowing to transversally move the sample with respect to the pump beam and to the cavity optical axis. This feature was exploited to check the uniformity of the laser output across the sample clear aperture, as it will be discussed below.
The pump output was modulated with square pulses, at 10 Hz repetition rate, and variable duty factors (from 20% to CW). In this way we were able to study the behavior of the samples under different levels of thermal load.
In order to properly evaluate the absorbed pump power we monitored the power of the residual pump beam transmitted by the sample with an auxiliary power monitor placed behind the folding mirror FM. The correction for the Fresnel reflection at the crystal interfaces was also properly applied. As it was pointed out in previous papers [14] the actual sample absorption in lasing conditions (that is under high pump and laser power density) is usually different from the unsaturated absorption , as it is influenced by two counteracting effects: on one hand the absorption saturation caused by the high pump power density (which reduces the power deposition into the sample), and on the other hand the rapid deexcitation of the lasing ions from the upper laser level to the ground level, which restores the population on the ground level and thus the absorption of the pump beam. The balance of these two effects depends both on the pump power density and on the laser intracavity power density, and thus on the transmission of the output coupler.

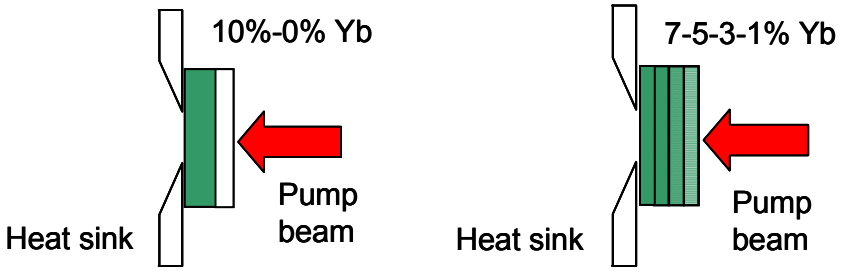

Figure 4 - Orientation of the doped layers with respect to the heat sink.

5. RESULTS

Slope efficiency measurements.

At first, we investigated the behavior of the samples under low thermal load, i.e. with quasi-continuous wave pumping (quasi-CW) with rectangular pump pulses at 10 Hz and a duty factor of 20% (that is, 20 ms pump on followed by 80 ms of pump off). We measured the output power from the different samples for increasing values of incident pump power, and we calculated the resulting lasing pump power threshold and slope efficiencies. All the samples lased at a wavelength of 1029.5 nm, in all the excitation conditions.

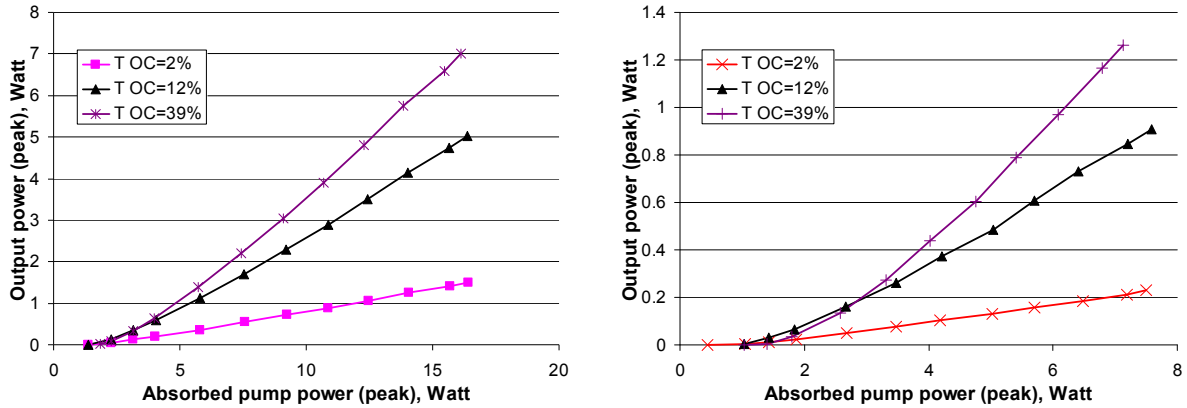

Figure 5 - Laser output behavior of the samples made by spray drying. Left: doping 0-10% Yb, right doping 1-3-5-7% Yb. TOC denotes the transmission of the output coupler. Color online.

Sample #	Doping structure	Absorption	Slope efficiency		
			TOC=2%	TOC=12%	TOC=36%
SD-1	0%-10%	75%	11%	38.3%	56.3%
SD-2	1-3-5-7%	34%	3.8%	16.1%	26.7%
TC-1	0-10%	40%	15.1%	43.3%	54%
TC-2	1-3-5-7%	43%	6.0%	17.1%	37.9%

Table 5 - Slope efficiency for different values of the output coupler transmission (TOC), for the samples with different doping profiles and fabrication process. Quasi-CW pumping with 20% of duty factor. SD: spray drying; TC: tape cast.

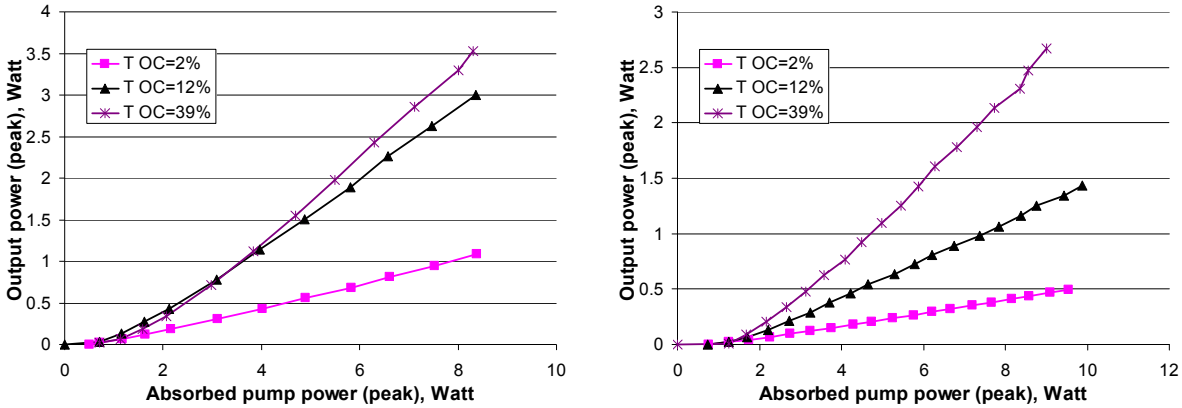

Figure 6 - Laser output behavior of the samples made by tape cast. Left: doping 0-10% Yb; right: doping 1-3-5-7% Yb. T OC denotes the transmission of the output coupler. Color online.

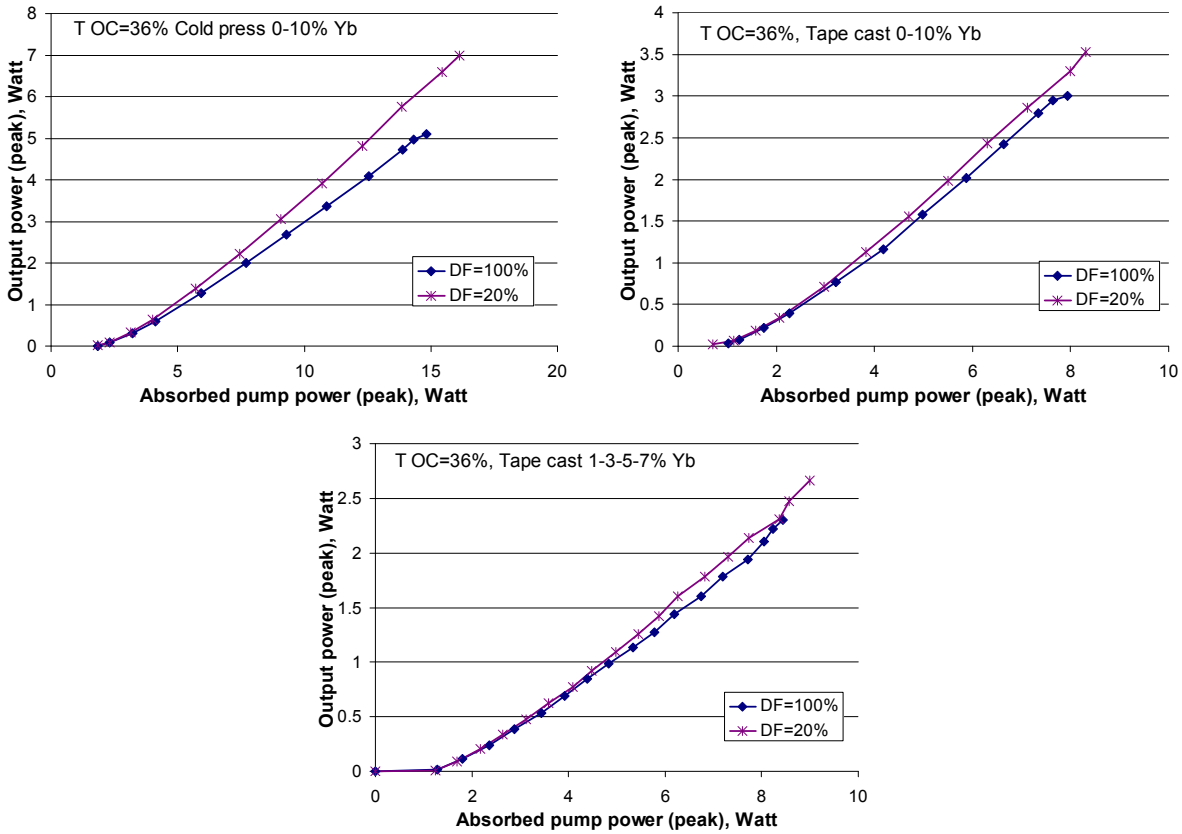

Figure 7 - Comparison of the laser output behavior for pump duty factor (DF) 20% and 100%, with TOC=36%. Doping profile and fabrication technique is specified in the graphs. Color online.

It must be noticed that the samples showed different overall pump absorption due to the different doping levels and structure. Therefore, in order to set a proper comparison among the samples, the results are reported as a function of the absorbed pump power. The graphs show the peak output power (i.e. the value of the output power obtained during the "pump on" periods) for increasing values of the absorbed pump power, for different values or the transmission of the output coupler. Figure 5 show the behavior of the samples fabricated by spray drying, with the two different doping profiles under investigation, *i.e.* stepped 10%-0% and graded 7-5-3-1%. The input-output curves for the samples fabricated by tape cast are shown in Figure 6.
The values of the pump absorption and of the slope efficiency for the various samples are reported in Table 5.
In order to evaluate the impact of the thermal load on the various doping geometries, we then characterized the input-output behavior in CW pumping regime. In this way we can investigate the effect of an increased thermal load, under the same instantaneous pump power level used in the previous measurements.
The measurements were carried out with T OC=36%, that is the output coupler that gave the better slope efficiency with all the samples under low thermal load. We excluded from this analysis the sample with graded doping, made by spray drying, which gave the poorest performance under quasi-CW excitation. The results are shown in Figure 7.

Characterization of the sample uniformity

The spatial uniformity of the ceramic samples is also an issue, in particular in view of the development of large laser active elements for high energy laser sources.
In order to have an insight of the impact of the internal defects of these samples on the uniformity of the laser performance, we have mapped the laser output on different positions of the sample.
For this purpose, the sample holder (which has a clear aperture of 3 mm) was moved by a micrometric translation stage, along a transect perpendicular to the cavity axis, in steps of 100μm. For each position of the sample we recorded the laser output with TOC=36%, under low thermal load conditions (20% duty factor). The overall cavity alignment remained unperturbed by this operation.

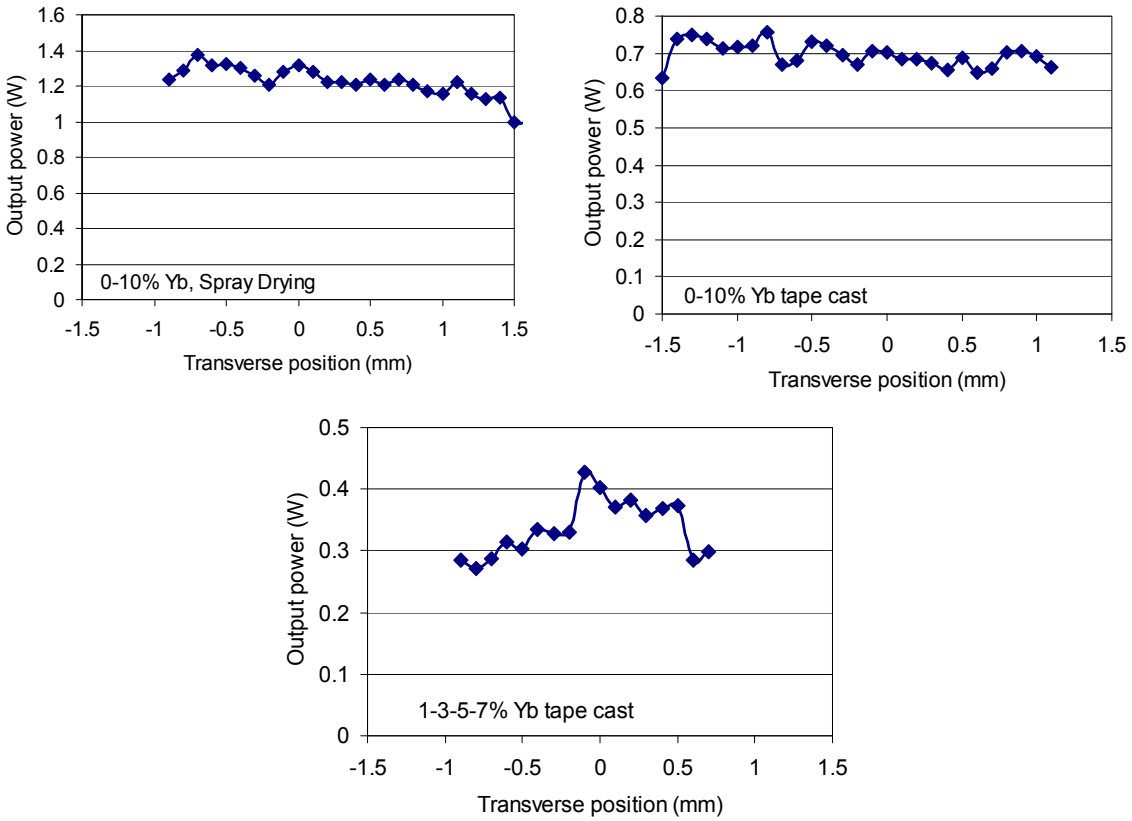

Figure 8 - Variation of the output power for different positions of the sample, moved perpendicularly to the cavity axis. The relative variation (standard deviation) is 6.4% for the sample with 0-10% doping made by spray drying, 4.5% for the sample with 0-10% doping made by tape cast, and 13.7% for the sample with the graded doping profile made by tape cast.

The fluctuations in the output power are due to small scattering defects that crosses the lasing region of the sample and induce scattering losses. Due to the relatively large size of the pump beam, the output power fluctuations are mostly due to large, unevenly distributed defects, rather than to small, uniformly distributed defects.
It can be seen (Figure 8) that in this case the sample with the smallest relative fluctuations was the one with the stepped doping profile made by tape cast (4.5% of standard deviation in the output power with respect to the average along the whole transect). The sample with the largest fluctuation (e.g. larger sparse defects) was the one with the graded doping distribution.

6. DISCUSSION

From the analysis of the results exposed above, it appears that both the spray drying and the tape cast techniques are capable to produce samples with a quite high slope efficiency (around 54-56% for the most favorable output coupling condition), as long as a small number of individual layers with different doping is used, as in the case of the samples with 0-10% doping profile.
In the samples under investigation, the increase of the number of layers (i.e. more complex structuring) is correlated with a reduction in the slope efficiency. This occurs for every value of the output coupling conditions, both for the samples fabricated by tape casting and by spray drying.
It can be seen that the sample with the stepped doping profile has shown a rather high slope efficiency (56.3%) under optimum coupling conditions. Conversely, the sample with the graded doping profile has a much smaller slope efficiency, for each value of the transmission of the output coupler.
The difference in the efficiency is most probably due to the higher density of internal defects (pores, scattering centers) in the sample with graded doping, whereas thermal effect should not have a relevant impact because the overall thermal load is low, thanks to the low pump duty factor. Indeed the differences in efficiency are consistent with the results of the test of internal homogeneity shown in Figure 8: the two samples with the highest slope efficiency (the 1-10% Yb made by tape cast and the 0%-10% Yb made by spray drying) show a similar internal homogeneity, with a relatively uniform laser output. On the other hand the sample with 1-3-5-7% doping made by tape cast, which ranked third in terms of slope efficiency, also shows the poorest internal homogeneity with the largest laser power fluctuations versus position.
Regarding the behavior under increasing thermal load, the samples made by tape cast have shown a more stable behavior than the sample made by spray drying. This is true in particular for the sample with stepped doping profile (0%-10% Yb), which shows an almost constant slope efficiency for increasing pump duty factor, whereas the sample with the same doping geometry made by tape cast shows a small decrease in slope efficiency when passing from QCW to CW pumping regime. It is interesting to note that also the sample made by tape cast with 1-3-5-7% doping has a rather stable behavior under increasing thermal load, even though its overall efficiency is affected by the higher density of internal defects.

7. CONCLUSIONS

The results of this work demonstrate that the tape casting technique is an useful technique for the production of ceramic samples with structured internal doping distribution. Indeed, the results in terms of laser efficiency and stability under high values of thermal load are well comparable with those obtained by well assessed techniques, in particular by means of thermal compression of spray dried powders. Tape cast is then a technique worth to be investigated and further perfected, because it is more flexible and less complicated than other forming techniques, in particular for the fabrication of complex structures made of several thin layers.
At the current level of development, the fabrication of multi-layered structures is still made difficult by the fact that increasing number of layers also increases the number and density of defects. This in turn results in relatively high scattering losses and poor samples internal homogeneity. It is worth to note that this problem occurs both whit the tape cast and with the thermal compression technique, i.e. it is not strictly related to the sample forming technique.
The numerical simulations here reported show that lasing elements featuring a graded doping distribution should be subjected to lower internal thermomechanical stress and lower peak temperature values. This in turn should make them more capable to accept higher pump power density levels, with respect to structures with stepped doping profiles.
Nonetheless, at the current level of development it is difficult to provide an experimental verification of these positive features, because the laser performance itself is currently strongly affected by the density of internal defects, which in turn is correlated with the number of layers. This introduces an undue bias in the comparison, which favors the overall laser performance of samples with a simpler layer structure.

Our next steps will then be aimed to improve the fabrication of multilayer structures, as a prerequisite for the development of the full potential of the internal doping structuring.

ACKNOWLEDGMENTS

We acknowledge support from the following projects:
- the EC initiative "LASERLAB-EUROPE" (EC contract no.284464) - Joint Research Activity WP33 - "European Research Objectives on Lasers for Industry, Technology and Energy (EURO-LITE)"
- the Flag project RITMARE, La Ricerca Italiana per il Mare – coordinated by CNR and funded by the Ministry of Education, University and Research within the National Research Program 2011-2013
- the HiPER (ESFRI-FP7) project. -
- P. F. would also like to acknowledge the financial support from Regione Toscana through the project "R&D of innovative wavefront sensors and Adaptive Optics for laser-driven Radiological Devices – AdOpRad" (protocollo ISTI-CNR No. 0000745, 09/03/2012).
- J. H. would like to acknowledge the support from specific university research (MSMT No 20/2015).

REFERENCES

[1] Nakamura, S., Yoshioka, H., Matsubara, Y. , Ogawa T. , Wada S., "Broadly Tunable Yb^{3+}-Doped $Y_3Al_5O_{12}$ Ceramic Laser at Room Temperature," Jpn. J. Appl. Phys. 48, 060205-1-060205-3 (2009)
[2] Esposito L., Piancastelli A., Costa L., Serantoni M., Toci G., Vannini M., "Experimental features affecting the transparency of YAG ceramics," Opt. Mat. 33 (5), 713 (2011)
[3] Pirri, A. , Alderighi D., Toci G., Vannini, M. "High-efficiency, high-power and low threshold Yb^{3+}:YAG ceramic laser," Opt. Express 17 (25), 23344 (2009)
[4] Kaminskii, A. A. , Akchurin, M. Sh., Gainutdinov, R. V., Takaichi, K., Shirakava, A., Yagi H., Yanagitani T., Ueda K., "Microhardness and Fracture Toughness of Y_2O_3- and $Y_3Al_5O_{12}$-Based Nanocrystalline Laser Ceramics," Crystallog. Rep. 50, 869 (2005).
[5] Ferrara, P., Ciofini, M.,. Esposito, L, Hostaša J., Labate L., Lapucci A., Pirri A., Toci G., Vannini M., Gizzi L. A., "3-D numerical simulation of Yb:YAG active slabs with longitudinal doping gradient for thermal load effects assessment," Opt. Express, 22, 5, 5375 (2014)
[6] Mistler, R. E. , Twiname, E. R. [Tape Casting: Theory and Practice], Westerville, USA, John Wiley & Sons, ISBN 978-1-57498-029-5 (2006)
[7] Esposito, L., Epicier, T., Serantoni, M., Piancastelli, A., Alderighi, D., Pirri A., Toci G., Vannini M., Anghel S., Boulon G., "Integrated analysis of non-linear loss mechanisms in Yb:YAG ceramics for laser applications," J. Eur. Ceram. Soc., 32, 2273-2281 (2012).
[8] Hostaša, J. , Esposito L., Piancastelli, A., "Influence of Yb and Si content on the sintering and phase changes of Yb:YAG laser ceramics", J. Eur. Ceram. Soc., 32, 2949 (2012).
[9] COSMOS M, Design Star Product, Structural Research and Analysis Corp. – (User's Guide and Tutorial), www.cosmosm.com , Los Angeles, 2001.
[10] Lapucci, A.,Ciofini, M., Esposito, L. , Ferrara, P. , Gizzi, L. A. , Hostaša, J. , Labate, L., Pirri, A. , Toci, G. , Vannini M., "Characterization of Yb:YAG active slab media based on a layered structure with different doping," Proc. of SPIE Vol. 8780, pp. 87800J-1,87800J-12, 2013.
[11] Chénais, S., Druon, F., Forget, S., Balembois, F., Georges, P. "On thermal effects in solid-state lasers: The case of ytterbium-doped materials," Progress in Quantum Electronics 30 (4), 89–153, (2006).
[12] Koechner, W., Rice, D. K., "Effect of birefringence on the performance of linearly polarized YAG: Nd lasers," IEEE J. Quantum Electron. 6(9), 557–566 (1970).
[13] Khazanov, E. A., "Thermally induced birefringence in Nd:YAG ceramics," Opt. Lett., 27(9), 716-718, (2002).
[14] Pirri, A. , Alderighi, D., Toci, G., Vannini, M. , Nikl, M., Sato, H. "Direct Comparison of Yb^{3+}:CaF_2 and heavily doped Yb^{3+}:YLF as laser media at room temperature," Opt. Express **17**, 18312-18319 (2009)